Journal of Colloid and Interface Science 557 (2019) 357–366

Contents lists available at ScienceDirect

Journal of Colloid and Interface Science

journal homepage: www.elsevier.com/locate/jcis

Molecular-scale investigation of fluoride sorption mechanism by nanosized hydroxyapatite using ^{19}F solid-state NMR spectroscopy

Chao Ren [a,b], Zhiwu Yu [c], Brian L. Phillips [d], Hongtao Wang [a], Junfeng Ji [a], Bingcai Pan [b], Wei Li [a,b,*]

[a] Key Laboratory of Surficial Geochemistry, Ministry of Education, School of Earth Sciences and Engineering, Nanjing University, Nanjing 210023, China
[b] Research Center for Environmental Nanotechnology (ReCENT), Nanjing University, 210023, China
[c] High Magnetic Field Laboratory, Hefei Institutes of Physical Science, Chinese Academy of Sciences, 350 Shushanhu Road, Hefei 230031, China
[d] Department of Geosciences, SUNY Stony Brook, Stony Brook, NY 11794-2100, United States

GRAPHICAL ABSTRACT

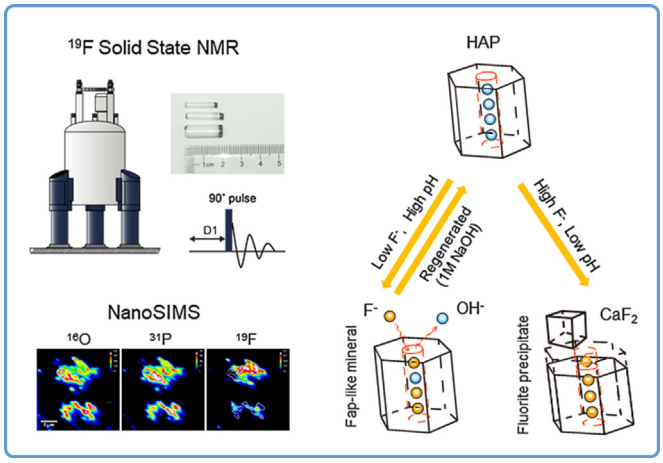

ARTICLE INFO

Article history:
Received 22 July 2019
Revised 10 September 2019
Accepted 11 September 2019
Available online 12 September 2019

Keywords:
Hydroxyapatite
Fluoride
^{19}F NMR
Sorption
Dissolution-precipitation
Regeneration

ABSTRACT

Hydroxyapatite (Hap) has been shown to be an excellent sorbent for F^- removal of elevated levels of fluoride in groundwater worldwide; however, the molecular mechanisms of this process have not been clearly addressed. Herein, we used ^{19}F solid-state NMR spectroscopy to investigate F^- sorption mechanisms by nanosized Hap combined with ^1H NMR and $^1H\{^{19}F\}$ Rotational Echo DOble Resonance (REDOR) technology in addition to other characterization methods such as Transmission Electron Microscopy (TEM), X-ray Diffraction (XRD) and Nanoscale Secondary Ion Mass Spectroscopy (NanoSIMS). Our experimental results showed that F^- sorption mechanisms depend on solution pH and fluoride concentration ($[F^-]$). At pH 7 and $[F^-] \leq 50$ mM, a single ^{19}F NMR peak at −103 ppm was observed, which could be assigned to fluorapatite $[Ca_5(PO_4)_3F]$ (Fap) or fluoro-hydroxyapatite solid solution $[Ca_5(PO_4)_3F_x(OH)_{1-x}; x = 0–1]$ (F-Hap). A simultaneous formation of fluorite (CaF_2) precipitates (δ_{F-19} = −108 ppm) was observed at higher $[F^-]$ (e.g., 100 mM), which was further confirmed by TEM and XRD analysis. The NanoSIMS and $^1H\{^{19}F\}$ REDOR analyses indicated that a dissolution-precipitation pro-

* Corresponding author at: Key Laboratory of Surficial Geochemistry, Ministry of Education, School of Earth Sciences and Engineering, Nanjing University, Nanjing 210023, China.
E-mail address: liwei_isg@nju.edu.cn (W. Li).

https://doi.org/10.1016/j.jcis.2019.09.039

cess was involved in the F^- sorption on Hap. Our results strongly support the efficacy of Hap for F^- removal even after several instances of regeneration, making it a cost-effective strategy for fluoride treatment.

1. Introduction

Fluoride (F^-) is a widespread contaminant in both groundwater and drinking water [1]. Globally, there are more than 25 countries and districts and more than 200 million people that suffer from fluorosis in tooth and bone [2,3], which is caused by unsafe drinking water containing F^- above the World Health Organization (WHO) standard concentration (i.e., 1.5 mg/L or 79 μM) [4,5]. In developing countries (e.g., China, India), adsorption-based techniques are effective strategies that have been widely adopted due to low-cost, simple design and convenience of operation [1]. Many adsorbents have been successfully applied in defluoridation schemes including activated alumina [6], zeolites [7], bone char [8], active carbon [9], calcite [10], clay [11], bleaching clay [12] and red mud [13]. Recently, considerable attention has been paid to the use of bone charcoal (with the major component as hydroxyapatite [$Ca_5(PO_4)_3OH$] (Hap)), which is widely used in developing countries for defluoridation due to low cost, strong sorption ability, excellent performance, and environmental compatibility [14–16]. Although previous studies have extensively investigated macroscopic sorption behavior and the effect of variables such as reaction time, dosage and pH [14,17,18], the molecular mechanisms of the interaction between F^- and the surface or the unidimensional channels of the crystal structure of Hap (Fig. 1) remain poorly understood. Although the formation of fluoridated Hap has been suggested in some studies, direct experimental evidence is still lacking. Debates have mainly centered on the possible products formed among the fluoro-hydroxyapatite solid solution [$Ca_5(PO_4)_3F_x(OH)_{1-x}$; x = 0–1] (F-Hap), fluoridated Hap with the thin fluorapatite [$Ca_5(PO_4)_3F$] (Fap) layer and a separate Fap phase. Moreover, when fluorite (CaF_2) precipitates at specific conditions, which is important for industrial defluoridation, remains unknown.

Because F is a light element, characterizing its molecular information is challenging. To elucidate the F^- uptake mechanism by Hap, structural characterization methods such as powder X-ray diffraction (XRD) and Fourier transform Infrared (FTIR) have been employed [14,17,19], but neither could provide sufficient information to characterize both surface adsorption and precipitation. XRD can detect newly formed crystalline secondary precipitates (e.g., CaF_2) but is not sensitive to precipitates that are amorphous or crystalline with low content (e.g., <3% by weight). Furthermore, XRD fails to characterize surface adsorbed F^- lacking long-range structural order. FTIR spectroscopy is a technique that is sensitive to short-range-ordering structure, especially the coordination environment and symmetry of relevant molecular groups (e.g., CO_3, PO_4, OH) [20]. Therefore, FTIR can characterize (OH, F) structural ordering in the F-Hap solid solution series and has been used to indirectly estimate the F content in Hap structural tunnels after F^- uptake [19]. However, it cannot detect CaF_2 precipitates because ionic compounds (e.g., CaF_2, KBr) yield no IR signal. Very recently, Nano Secondary Ion Mass Spectroscopy (NanoSIMS) and synchrotron F *K*-edge X-ray Absorption Near Edge Spectroscopy (XANES) have been applied to investigate the mechanisms of F^- sorption by nano-Hap [19,21], but both techniques have limitations related to the simultaneous quantification of surface adsorbed F^- and CaF_2 precipitates. Furthermore, both require expensive instrumentation and facilities that are not widely available.

In principle, ^{19}F nuclear magnetic resonance (NMR) spectroscopy is a well-suited tool to probe the F^- sorption mechanism at mineral/aqueous solution interfaces for several reasons. First, ^{19}F has nuclear spin I = ½ and a 100% natural abundance, which contributes to high sensitivity and simplicity in spectral interpretation. Second, the ^{19}F chemical shift is very sensitive to the chemical environment at the molecular scale, which could allow resolution of distinct F species (e.g., adsorption complexes as well as any Ca-fluoride precipitates) [22–24]. Several early studies in dentistry used NMR to study F^- adsorption on Hap at physiological conditions (i.e., neutral pH, 37 °C) [24]. These results suggest that F-substituted Hap and CaF_2 precipitates could be distinguished

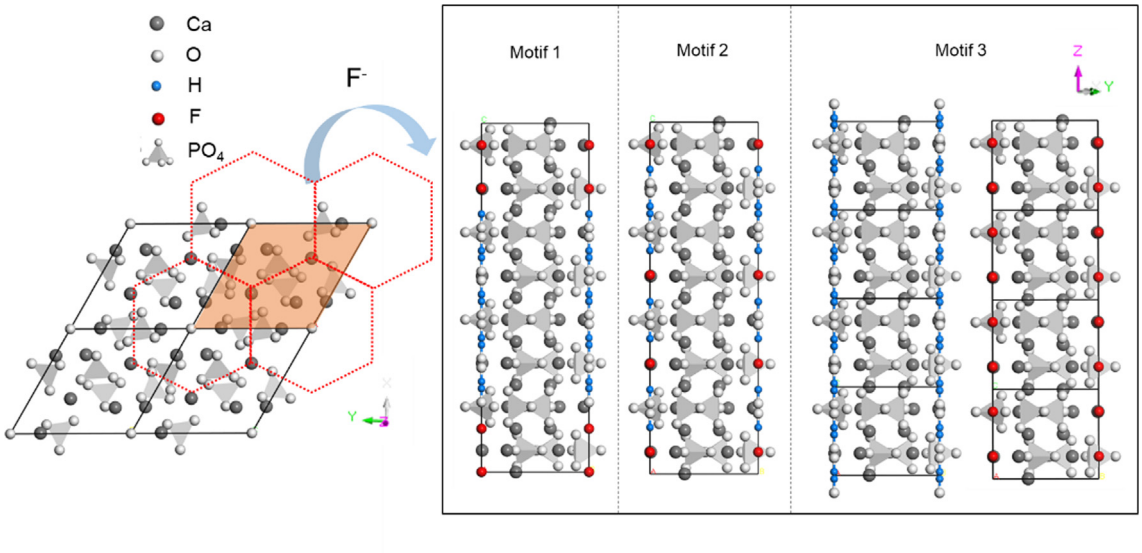

Fig. 1. Crystal texture of Hap in the view of the c-axis (left) and possible F^- arrangement after reaction with Hap.

by their chemical shift. However, early NMR techniques only allowed a low spinning rate (e.g., 3 Khz) resulting in a very broad peak for the CaF_2 signal and caused large uncertainties in quantification, leading to a poor understanding as to why F^- can substitute to the tunnel OH^- group in Hap and under which conditions CaF_2 precipitates can form. This limitation can be improved by the use of high-speed magic angle spinning (MAS) instrumentation. Additionally, a wide range of double resonance NMR methods are now available that can probe spatial proximity between ^{19}F and ^{1}H (e.g., REDOR, short for Rotational Echo DOuble Resonance). Furthermore, the sensitivity of current NMR spectrometry was greatly improved to allow the measurement of samples with low concentrations comparable to a realistic environment.

Here, we present a ^{19}F solid-state NMR study on F^- sorption by Hap to elucidate the reaction mechanisms. To complement the NMR analysis, a combination of XRD, FTIR, NanoSIMS, and High Resolution-Transmission Electron Microscope (HRTEM) were also applied. The objectives of this study were to reveal and delineate the mechanism of F^- sorption with respect to environmental factors and to provide a better understanding of the application of low-cost apatite material for F^- removal in groundwater remediation.

2. Materials and methods

2.1. Reagents and standards

Nanosized Hap was purchased from Sinopharm Chemical Reagent Co., Ltd. and contained no impurities detectable by powder XRD, SEM and TEM analysis (see Figs. S1 and S2). The Hap had a specific surface area of 15.2 $m^2 \cdot g^{-1}$ according to a BET-N_2 measurement with an Autosorb-1 standard physical adsorption analyzer (Quantachrome Autosorb-1, Boynton Beach, FL). The synthesis of Fap followed the method described by Sternitzke et al. [19]. A standard specimen of fluorite was obtained from the Nanjing University Mineral Collection.

2.2. Sorption experiments

Sorption experiments were conducted in static batch experiments at ambient temperature 25 (±1) °C. All solutions were made with ultrapure deionized water with resistivity >18.2 MΩ cm. A 0.100 g aliquot of Hap powder was added to a 40 mL of solution that contained 0.01 M NaCl background electrolytes [25]. Solution pH was controlled through all sorption experiments and adjusted by slow addition of 0.01 M HCl or NaOH to reach the desired range (±0.1). A series of experiments were designed and performed in duplicate to examine the effects of environmental factors (i.e., time, concentration, pH, and regeneration). Batch experiments were carried out at fluoride concentrations of 0.5 and 1 mM from 15 min to 48 h at various pH values from 4 to 10, where F^- is the dominant aqueous species (Fig. S3). Detailed chemical thermodynamic analysis on the speciation of aqueous species and the stability of solid phases are provided in the Supplementary information (Figs. S3 and S4, Table S1).

Sorption isotherms were conducted at initial F^- concentrations ranging from 0.05 to 500 mM at a specific pH for 48 h. To investigate the sustainable application of nanosized Hap, regeneration experiments were performed (Scheme 1). After the sorption experiment with 0.5 mM initial F^-, Hap was immersed into a 1 M NaOH solution and agitated at 120 rpm on a rotary shaker for 2 h. Products were centrifuged and filtered with a 0.22-μm membrane filter to separate the solid from suspension. The solids were reused for subsequent sorption experiments. Four cycles of regeneration experiments were conducted.

After reaction, the samples were centrifuged to separate the solid and solution with the supernatant filtered by a 0.22-μm membrane filter. The concentration of fluoride ions in the supernatant was determined using an Alalis pH-400 m equipped with a fluoride ion selective electrode (ISE) with a detection limit of 10^{-6} M. A 50% TISAB (Total Ionic Strength Adjustment Buffer) was added to all fluoride standards to maintain a certain pH (5–6) to ensure a consistent electrode response for F^- measurements [18,24]. The solids were rinsed with ultrapure deionized water and air-dried for further XRD, NMR, FTIR and TEM characterization. Details of XRD and FTIR analysis are provided in the supporting information.

2.3. HRTEM

Solid samples before and after the F^- sorption were analyzed by HRTEM. Small quantities of powdered reactants were dispersed in deionized water and ultrasonicated for 5 min. A few drops of this suspension were put through a 200 mesh Cu grid with a lacey-carbon support film and then dried. TEM analyses were made using a FEI Tecnai (F20) microscope at an accelerating voltage of 200 KeV, equipped with an Oxford light element Energy Dispersive X-ray spectroscopy (EDX) detector and a Gatan GIF 200 CCD imaging system. Both selected area electron diffraction (SAED) and EDX were performed on the F^- sorption samples. The point-to-point resolution of the TEM is better than 0.2 nm and the line resolution is 0.09 nm. Images were analyzed and processed using Gatan Digital Micrograph 1.8 software. The software package ES Vision4 was used to acquire and process the EDS spectra.

2.4. Solid-State NMR

Solid-state ^{19}F single-pulse (SP)/magic angle spinning (MAS) NMR spectra of F^- sorbed Hap were performed on a 600 MHz Bruker Advance II spectrometer (14.1 T) at an operation frequency of

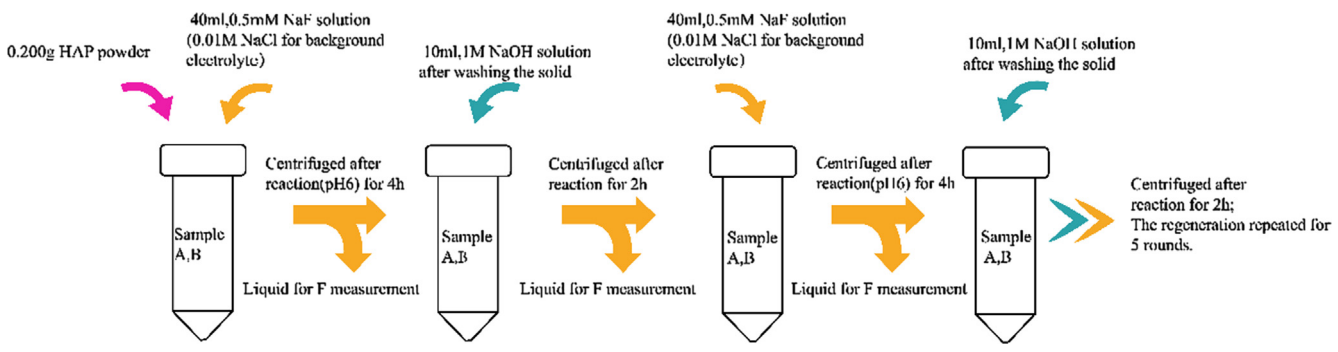

Scheme 1. Regeneration procedure of Hap after use as a sorbent for removal of fluoride; sample A and B are for comparison.

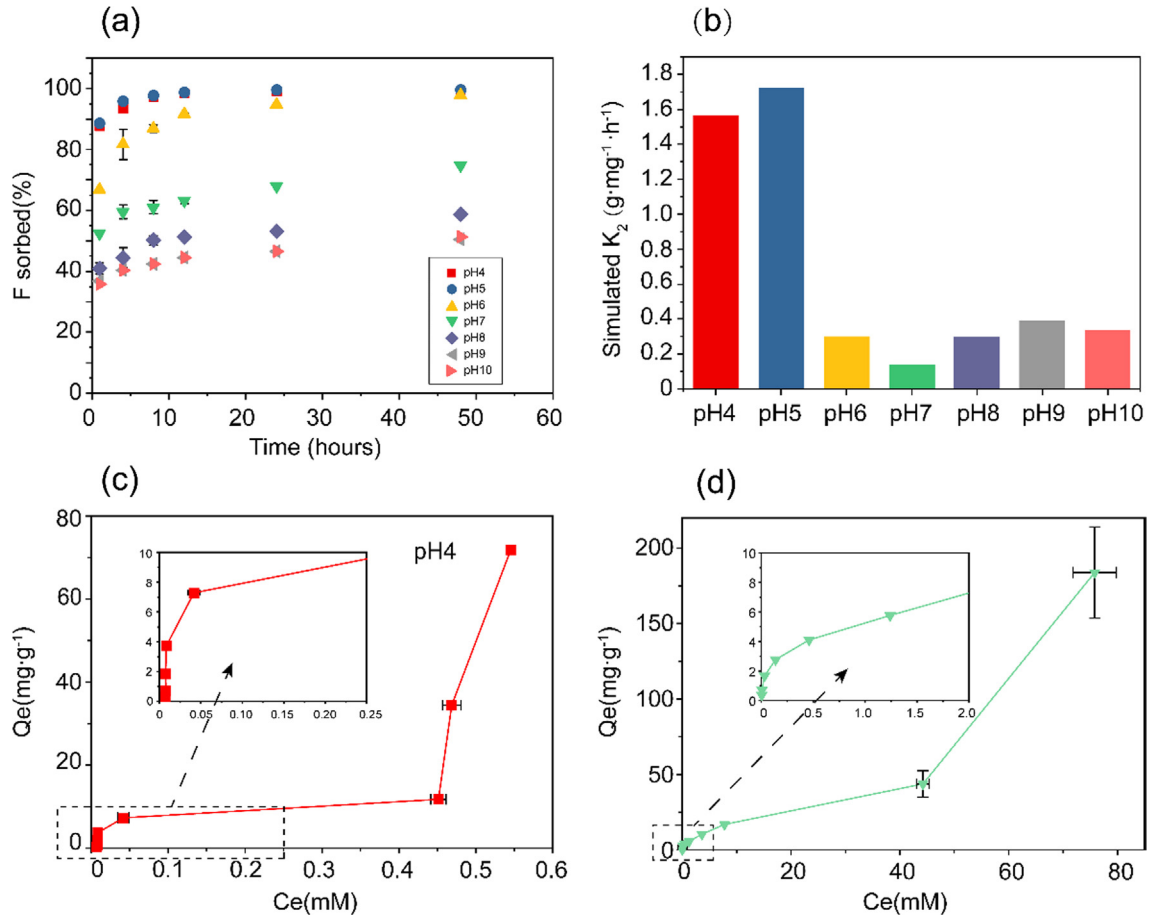

Fig. 2. Uptake of fluoride by hydroxyapatite (Hap): sorption kinetics at several pH values (pH 4–10) with a 0.5 mM F^- initial concentration (a), equilibrium rate constant K_2 simulated from pseudo-2nd order sorption model (R^2 = 0.99) (b). Uptake of F^- by Hap as a function of F^- initial concentrations ranging from 0.05 – 10 mM at pH 4 (c) and 0.05–100 mM at pH 7 (d). Insets in (c) and (d) display uptake curves at a narrow F^- concentration range that are well fitted with the Freundlich isotherm mode.

564.5 MHz. Spectra were collected using a H/F/X CP-MAS probe with samples contained in 4.0 mm (o.d.) normal wall ZrO_2 rotors at room temperature. Spectra were obtained at a spinning rate of 14 kHz with an excitation π/6 pulse of 2 μs using a 30 s repetition delay. The spectra taken for some samples at a longer delay showed no further increase in absolute intensity. The ^{19}F chemical shifts ($\delta_{F\text{-}19}$) were modified by a $CFCl_3$ reference ($\delta_{F\text{-}19}$ = 0 ppm). Approximately 500–1000 scans were collected for each sample to obtain a reasonable signal-to-noise ratio.

The ^1H SP/MAS spectra were collected on a 400 MHz Bruker Advance III spectrometer (9.4 T), at operating frequencies of 399.8 MHz for ^1H. The ^1H SP/MAS spectra were obtained at a π/2 pulse of 2 μs, 5 s repetition delay, and spinning rates of 20 kHz. The ^1H chemical shifts ($\delta_{H\text{-}1}$) were set by a reference of adamantine ($\delta_{H\text{-}1}$ = 1.8 ppm).

$^1H\{^{19}F\}$ REDOR spectra were obtained on a 400 MHz Bruker Advance III spectrometer (9.4 T) operating at 399.8 and 376.5 MHz for ^1H and ^{19}F, respectively. Spectra were collected using a H/F/X CP-MAS probe with samples contained in 3.2 mm (o.d.) normal wall ZrO_2 rotors at room temperature. NMR signals were recorded under two conditions, one with ^1H π pulses of 4 μs and the other without π pulses (full spin-echo signal). The difference in signal arising only from the ^{19}F coupled to ^1H was obtained by subtracting the REDOR (S) from the spin-echo (S_0). The ^{19}F spin-echo spectra were obtained at spinning rate of 14 kHz with an excitation π/2 pulse of 3 μs and π pulse of 6 μs, using a 30 s repetition delay.

2.5. NanoSIMS

A Cameca Nano Secondary Ion Spectrometer (NanoSIMS) at the Institute of Geology and Geophysics, Chinese Academy of Science in Beijing was configured to measure the elemental distribution on the Hap after reacting with 50 mM F^-. Oxygen (^{16}O), phosphorous (^{31}P) and fluoride (^{19}F) were detected simultaneously. An analysis area of 10 × 10 μm^2 (256 × 256 pixel) was rasterized by Cs^+ accelerating to 16 keV with a beam of ~1.8 nÅ. The dwell time was 10 ms/pixel and each image consisted of five frames with a total measurement time of more than 1 h. The software ImageJ was used to process and analyze the elemental mapping data.

3. Results and discussion

3.1. Macroscopic sorption experiments

Fig. 2a shows the kinetics of F^- sorption by Hap with 0.5 mM [F^-] at pH 4–10. At all pH conditions, the reaction was initially fast, with most F^- being removed from solution within the first hour, followed by a much slower process with continued F^- removal extending to 12–48 h, similar to the results reported by previous research [10,18]. Since F^- and OH^- have similar radii and electron charge, OH^- might compete against F^- for sorption sites. Therefore, pH has a significant impact on F^- sorption. Experimentally, the

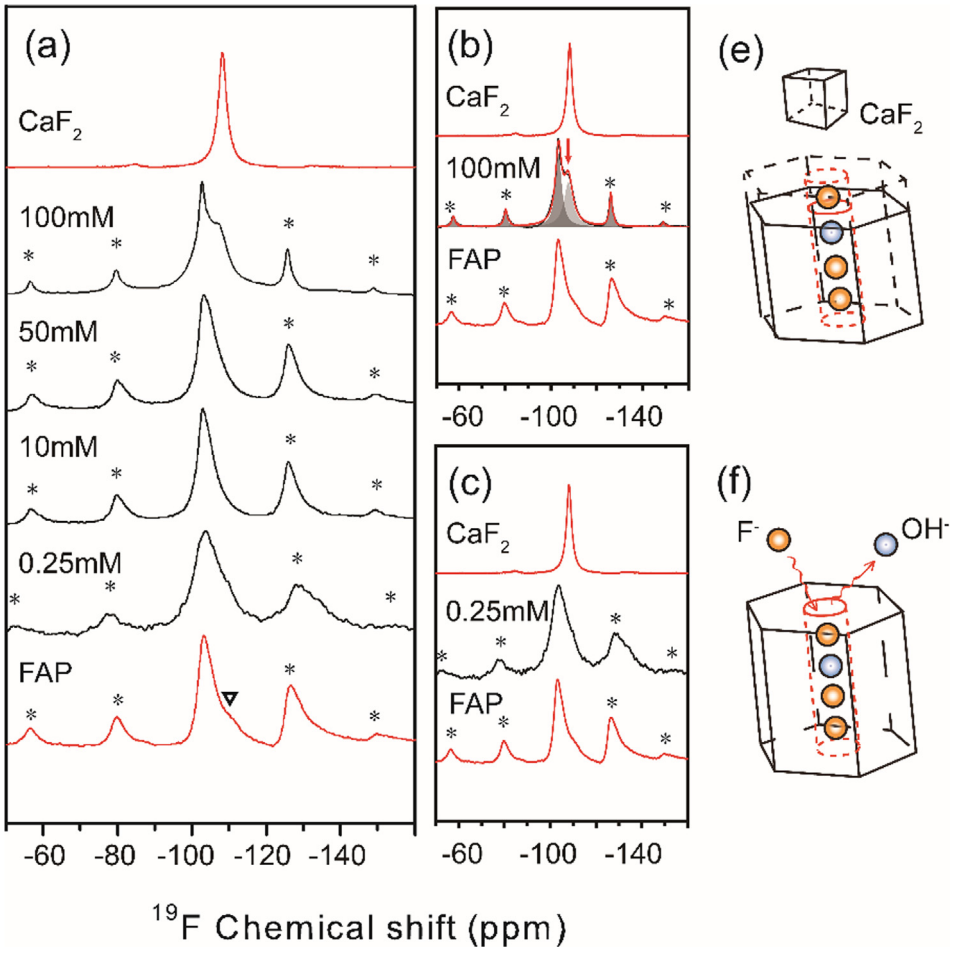

Fig. 3. ^{19}F SP/MAS NMR analysis for Hap samples reacted with various F^- initial concentrations from 0.25 mM to 100 mM and for fluorapatite (Fap, bottom) and fluorite (CaF_2, top) reference materials (a); a close inspection on the Hap reacted with 100 mM (b) and 0.25 mM (c); the cartoons representative for their corresponding reaction mechanisms (d)(e). NMR peaks at −103 ppm and −108 ppm are indicative of fluorapatite and fluorite. Spectra were acquired at a spinning rate of 14 kHz, with a π/6 pulse and a pulse delay of 30 s. Asterisks denote spinning sidebands and "▽" denotes CaF_2 impurities in the synthetic Fap.

sorption rate decreased drastically from 99.1% to 51.3% as pH increased from 4 to 10. Furthermore, we found that the pseudo-2nd-order sorption model ($R^2 \geq 0.99$) could best fit the F^- sorption kinetics. The fitted sorption rate constant K_2 from the pseudo-2nd-order sorption model reached a maximum as 1.5–1.7 $g{\cdot}h^{-1}{\cdot}mg^{-1}$ at pH 4–5, which decreased to a low level of 0.1–0.3 $g{\cdot}h^{-1}{\cdot}mg^{-1}$ at pH 6–10 (Fig. 2b), suggesting different rate-limiting steps according to acidic and alkaline conditions.

To quantitatively evaluate the sorption capacity, sorption isotherm experiments were performed at a larger concentration range, from 0.05 mM to 10 mM at pH 4 (Fig. 2c) and from 0.05 mM to 100 mM at pH 7 (Fig. 2d), respectively. At pH 4, the sorption isotherm appeared obviously different from the classic Langmuir- or Freundlich-type curves. At low $[F^-]$ (Fig. 2c, inset), the sorption curve could be fitted with the Langmuir model, yielding a maximum sorption of ~10 mg/g; but an abrupt transition occurred at the equilibrium concentration of 0.4–0.6 mM, with F^- sorption increasing almost linearly from 10.1 to 71.8 mg/g. A similar sorption curve was observed at pH 7 (Fig. 2d), where the Langmuir-like model could be applied only at low $[F^-]$ (0–50 mM) (Fig. 2c, inset). This rapid increase in sorption with extremely high sorption densities (e.g., 383 $F^-{\cdot}nm^{-2}$ for pH 7 and 100 mM $[F^-]$) likely suggested the possible formation of F-containing precipitates [26–28].

3.2. ^{19}F Solid-State NMR spectroscopy

The ^{19}F MAS NMR spectra (Fig. 3a) were acquired to explore the mechanisms for F^- sorption by Hap. At pH 7, samples prepared at $[F^-]$ ranging from 0.25 to 50 mM yielded the same strong peak at around −103 ppm with several spinning sidebands (noted by asterisks), suggesting a similar F^- sorption mechanism. This −103 ppm peak could be assigned to tunnel F in the apatite structure (Fig. 3e), based on the similarity of the chemical shift with that for synthetic Fap (Fig. 3c, Fig. S5) [29].

As the $[F^-]$ further increased to 100 mM, an additional peak appeared at a chemical shift of −108 ppm (noted by the red[1] arrow, Fig. 3b), which was identical to that for synthetic CaF_2 (Fig. S5). A least square fit of the NMR spectrum indicated that the −108 ppm peak accounted for 39% of the total NMR signal. At extremely high $[F^-]$ (e.g., 500 mM), the main peak at −108 ppm could be observed (Fig. S7e), indicating that formation of CaF_2 precipitates becomes the dominant mechanism for F^- sorption at a highly elevated concentration (Fig. 3d). The observation of CaF_2 precipitates by NMR spectroscopy is supported by results from TEM images, EDX and SAED analyses (Fig. S7a–d), as well as the powder X-ray diffraction analysis (Fig. S7f) by the appearance of peaks at 28.3°, 47.0° and

[1] For interpretation of color in Fig. 3, the reader is referred to the web version of this article.

55.8° 2θ which can be indexed to (1 1 1), (2 0 0) and (2 2 0) crystallographic planes of fluorite (CaF_2), respectively.

Although the formation of CaF_2 precipitates has been proposed previously in the dentistry literature [30], to the best of our knowledge the conditions for CaF_2 precipitation have never been constrained. A thermodynamic prediction of the dissolution of Hap (Fig. 4b) and subsequent formation of CaF_2 was calculated using MINTEQ version 3.1 (Fig. 4a, dashed line in grey). The details are provided in the Supporting Information. When pH is lower than 4.5, Hap fully dissolves which supplies plenty of Ca^{2+} for the precipitation of fluorite (Fig. 4b). As the pH increased from 4.5 to 10, the dissolution of Hap is inhibited, leading to an exponential increase in the F^- concentrations required for fluorite precipitation (Fig. S4b). However, theoretical simulation cannot predict mechanisms such as surface complexation or ion-exchange that have already been reported for some cations and anions because it is solely based on the dissolution-precipitation equilibrium theory and known solubility constants of different solids [31]. To clarify the formation conditions resulting in CaF_2 precipitation, a systematic ^{19}F solid-state NMR and XRD characterization (Figs. S6 and S8) were conducted with respect to a wide range of F^- concentrations (0.1–100 mM) and pH (4–10). The results are summarized in Fig. 4a. At neutral pH, it was found that the formation of CaF_2 precipitates occurred only when [F^-] reached a specific value (e.g. 100 mM at pH7). At [F^-] ≤ 50 mM, no precipitates could be detected using either ^{19}F NMR (Fig. S6b) and XRD (Fig. S8b). This finding explains why Sternitzke et al. did not observe CaF_2 precipitates during F^- sorption at nanosized Hap up to 7 mM (at neutral and slightly alkaline condition) [19], which are lower than the threshold concentration (i.e., 100 mM) suggested in the present study. Interestingly, at pH 4, a much lower threshold concentration (5 mM) would induce the formation of CaF_2 precipitates (Figs. S6a and S8a), consistent with previous research [32]. In contrast, at pH 10, CaF_2 precipitates did not form even at [F^-] up to 500 mM (Figs. S6c and S8c).

3.3. Formation conditions of the Fap-like sorption products

According to Fig. 4a, the formation of Fap-like products rather than CaF_2 precipitates is the dominant reaction mechanism for most natural groundwater (i.e., 0.05 mM < [F^-] < 10 mM; pH from 5.5 to 9). We performed systematic ^{19}F NMR analysis for samples prepared at a range of solution compositions that encompass these conditions (Fig. 5). These ^{19}F NMR spectra, for all samples prepared with [F^-] ranging from 0.05 mM to 10 mM at pH 7, contain a similar single peak at $\delta_{F\text{-}19}$ = −103 ppm (Fig. 5a), where the full-width at half maximum (FWHM) slightly decreased from 9.1 ppm for the 0.05 mM sample to 7.6 ppm for the 10 mM sample (Fig. 5c). The decrease in FWHM probably reflects changes in atomic ordering of the F substitution in the apatite structure [42]. With more F^- sorption, the arrangement of F^- becomes more ordered in the apatite tunnels, resulting in a narrower peak. Interestingly, it is worth noting that the 0.05 mM sample, which has the lowest F^- sorption, yields a $\delta_{F\text{-}19}$ of −103.2 ppm, which is ~0.2 ppm lower than that for Fap (Fig. 5a). More likely, there is a shoulder up field to that of Fap that is closer to CaF_2. Similar results are obtained for samples prepared at different pH values under the same [F^-] of 0.25 mM (Fig. 5b). As the pH decreased from 10 to 4, the FWHM of the ^{19}F NMR peak (−103 ppm) decreased linearly as a function of pH, from 11.6 ppm (pH 10, 0.25 mM) to 4.9 ppm (pH 4, 0.25 mM) (Fig. 5d). Coincidently, the pH 10 sample yielded a broad NMR peak comparable to that of the sample prepared at 0.05 mM and pH 7 with a similar chemical shift. Given that both samples contain very low sorbed F^- in which CaF_2 would not precipitate, we presume that F^- was adsorbed via binding the >Ca—OH sites on the surface of Hap or by substituting for OH at the tunnel sites near the Hap surface. Additionally, we observed a new signal at ~−95 ppm (noted as ▼) for 1 mM and 5 mM samples at pH 7 (Fig. 5a), which is assigned to carbonate fluorapatite (C-Fap) based on chemical shift or structural disorder that causes displacement of F^- away from the Ca^{2+} triangle in the Fap structure [43].

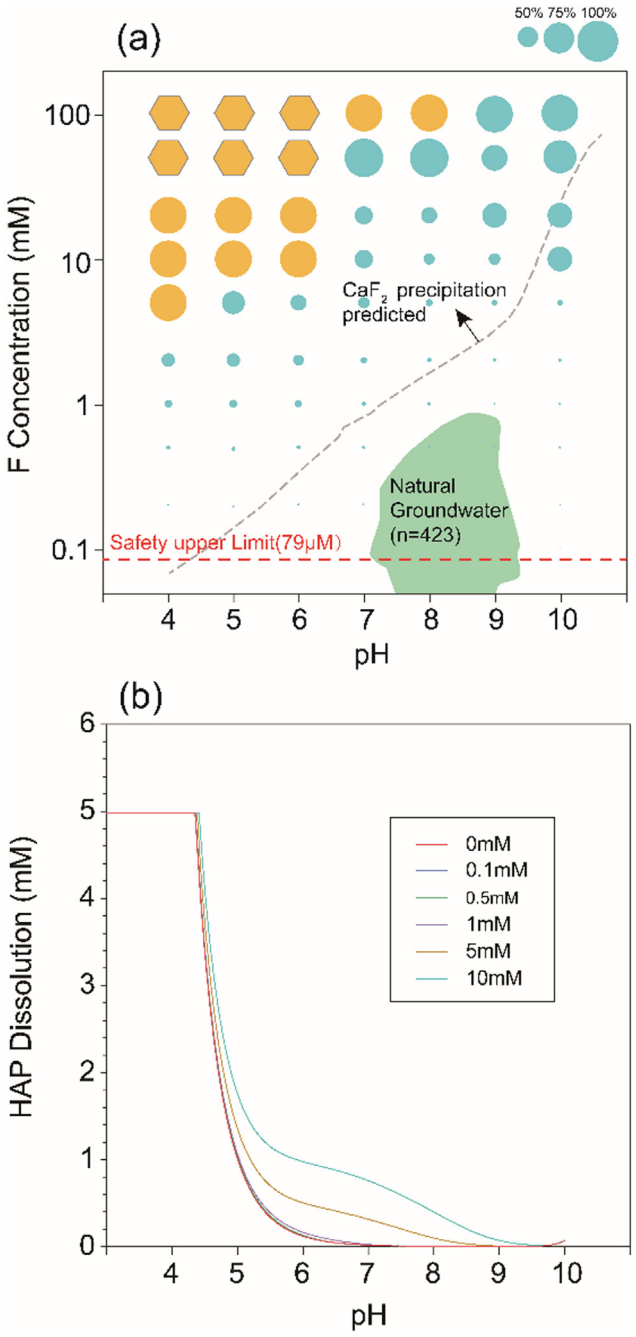

Fig. 4. (a) Summary of F^- uptake mechanism as a function of concentration (0.1–100 mM) and pH (4–10) according to MINTEQ calculation and ^{19}F NMR results. The gray dashed line represents the predicted conditions of F^- concentrations and pH at which fluorite could reach the saturation index and precipitate. The light blue circles represent the formation of F-Hap solid solution; the radii of the circles are proportional to the OH substitution rate by F^-; the yellow hexagons represent the formation of CaF_2 precipitates; the yellow circles represent a mixture of both. The F^- concentrations and pH ranges that the natural groundwater covers in the green region were collected from 423 data points according to Currell et al. [33]; He et al. [34]; Hu et al. [35]; Li et al. [36]; Salve et al. [37]. Smedley et al. [38]; Su et al. [39]; Vikas et al. [40]; Vikas et al. [41]; (b) Simulation of the dissolution of Hap with respect to solution pH without F^- by MINTEQ 3.1 version. (For interpretation of the references to colour in this figure legend, the reader is referred to the web version of this article.)

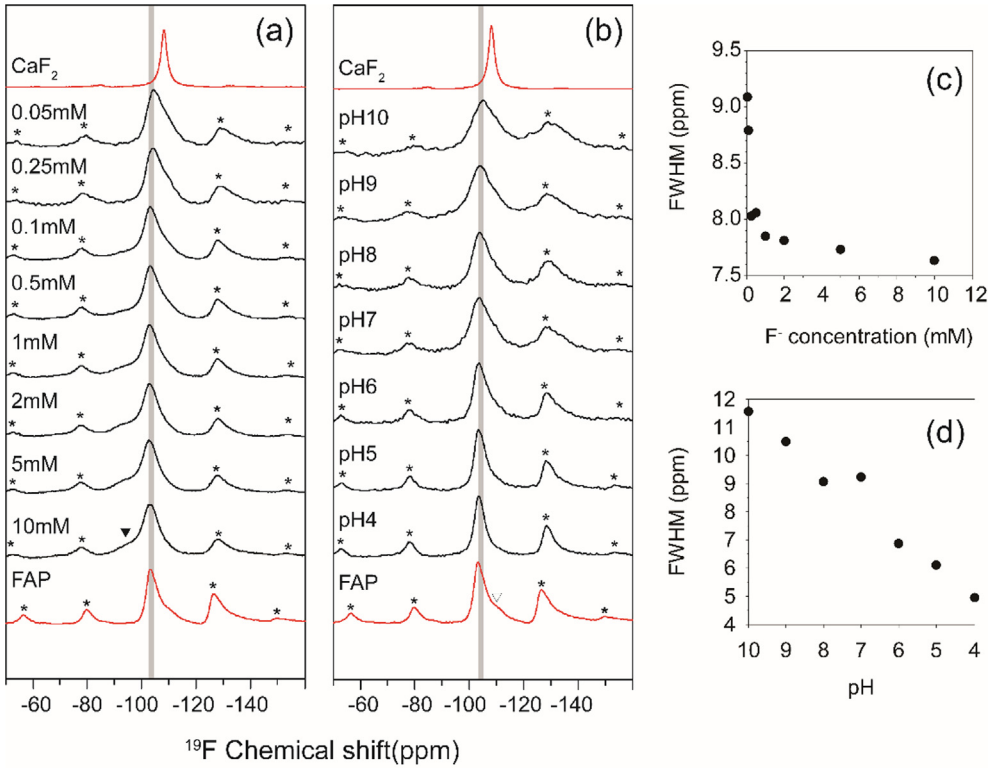

Fig. 5. ^{19}F SP/MAS NMR analysis for selected HAP samples reacted with varying initial F^- concentrations (from 0.05 to 10 mM) at pH 7 (a) and with varying pH (from 4 to 10) at an initial F^- concentration of 0.25 mM for 48 h (b). Spectra were acquired at a spinning rate of 14 kHz, with a $\pi/6$ pulse and a pulse delay of 30 s. Asterisks denote spinning sidebands. Spectra of reference samples including fluorite (top) and fluorapatite (bottom) are plotted for comparison, "▼" denotes carbonate fluorapatite phase, "▽" denotes fluorite, as aforementioned. The full width at half maximum (FWHM) of spectra in (a) and (b) are shown in (c) and (d) and are negatively correlated to the F/OH substitution rate.

To identify whether F located on the surface or in the bulk structure of Hap, ^{1}H NMR was applied and the occurrence of OH/F in the apatite tunnels was provided (Fig. 6). As shown in Fig. 6a, the peak intensity for $\delta_{H\text{-}1}$ = 0.2 ppm decreased gradually as F^- sorption increased. This peak has been assigned to the OH group, suggesting a decrement of OH—OH—OH motif in the Hap structure [23,29]. The broad peaks $\delta_{H\text{-}1}$ = 5.8 ppm for Hap and $\delta_{H\text{-}1}$ = 5.6 ppm for Fap are assigned to surface water [44]. The peak centered near 1.3 ppm become more pronounced with increasing F^- sorption. Although this peak has been tentatively assigned to the OH^- group related to F^- incorporation in the apatite structure [45,46], spectroscopic evidence is rarely investigated. In this study, ^{1}H{^{19}F} REDOR NMR experiments were performed to distinguish the specific H environment. Experimentally, two ^{1}H-observed NMR spectra were acquired including one (S) obtained with a heteronuclear dipolar dephasing sequence and a control spectrum (S_0) without irradiation at ^{19}F frequency. The difference in peak intensity ($\Delta S = S_0 - S$) depends on ^{1}H—^{19}F heteronuclear dipolar coupling and dephasing time. The difference spectrum yielded one peak at 1.3 ppm (Fig. 6b), suggesting H—F distance within 5 Å which could be definitely assigned to the OH^- group adjacent to F^- (i.e., OH—OH—F motif). The occurrence of the F—OH group was also confirmed by the FTIR analysis (Fig. S9, details provided in Supplementary Information 7). Interestingly, as [F^-] increased from 0.25 to 50 mM, the intensity of the 1.3 ppm peak in ^{1}H NMR (Fig. 6a) remained very weak similar to the REDOR difference spectra (Fig. 6b), suggesting that the H—F local structure is not widely distributed.

From our ^{19}F NMR results and the above discussion, we can propose three possible mechanisms for F sorption by Hap: (i) the formation of CaF_2 precipitates at high [F^-] and low pH, (ii) the formation of Fap [$Ca_5(PO_4)_3F$] or F-Hap solid solutions, and possibly (iii) the surface adsorption onto the surface of hydroxyapatite at the >Ca—OH sites.

3.4. New insights into the formation mechanism of Fap-like products

To clarify the existence of Fap precipitates, the NanoSIMS technique was applied (Fig. 7). Since both Hap and Fap phase contain structural PO_4^{3-} with an even part of them replaced by CO_3^{2-}, ^{16}O distribution can be used to constrain the particle boundaries in the NanoSIMS ions map. The distribution of ^{16}O is tightly correlated with ^{31}P in the colored contour (Fig. 7a and b). Surprisingly, the distribution of ^{19}F was heterogeneous (section 1 versus section 2, 3 and 4), suggesting distinct F-containing phases (Fig. 7c). ^{19}F is abundant in addition to ^{16}O and ^{31}P within particles in section 1 as highlighted by white solid lines, whereas it is deficient in section 2, 3 and 4. Combined with the differential distribution of ^{19}F and the solid-state NMR results, particles in section 2, 3 and 4 are likely to constitute a several nanometers thick 'fluoridated layer' on Hap, consistent with the previous findings of Sternitzke et al. [19].

While that the 'fluoridated layer' of Hap was confirmed, how it forms remains unclear. The formation of Fap during F^- sorption onto Hap has been extensively explained as an ion-exchange mechanism. This is mainly because substitution of F^- for OH^- in apatite structure is thought to be crystallographically stable, given that the size of the F^- ion (0.133 nm) is very close to that of OH^- (0.137 nm) [47]. As a result, F^- is located on the plane of three Ca^{2+} ions while OH^- is ca. 0.03 nm off the plane in the apatite structure [48,49]. However, observations of incongruent release of Ca^{2+} and PO_4^{3-} (i.e., $[Ca^{2+}]/[PO_4^{3-}] \approx 1.67$ in theory) in bulk solution were reported by several studies) [26], which seemed not to support the ion-exchange mode. Furthermore, the F profile was reported to be only several nanometers (i.e., 6 nm) on Hap, and F^- cannot diffuse any further into the tunnel sites due to the limited tunnel space and strong OH—F hydrogen bonding in the structure [49]. Surprisingly, in our study, we found that nearly 40 mg/g F^- sorption was reached and ~100% F substitution

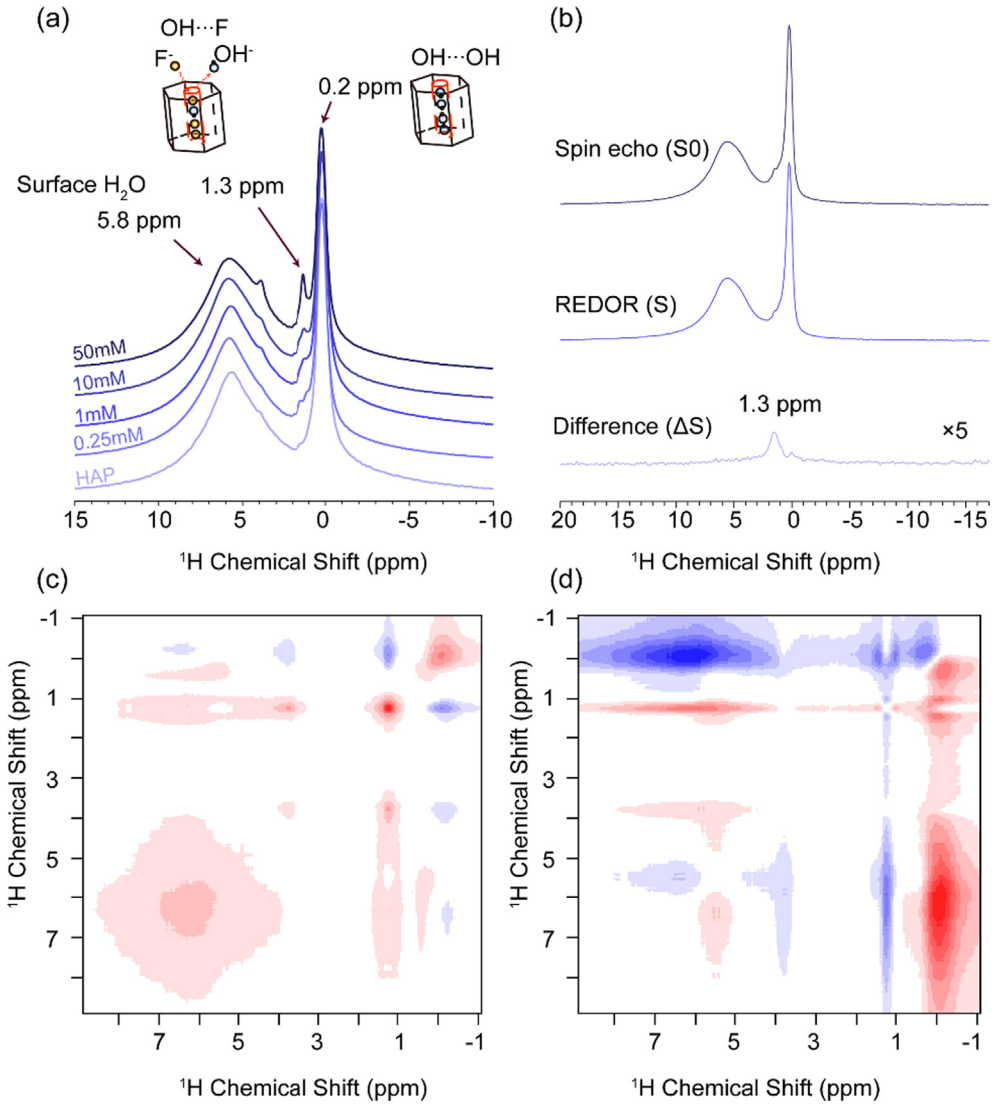

Fig. 6. ^{1}H SP/MS NMR of Hap before and after reaction with 0.25, 1, 10, and 50 mM F^{-} at pH 7 (a) with cartoons representing the relative local structure of protons (OH···OH and OH···F). ^{1}H{^{19}F} REDOR spectra analysis of Hap reacted with 50 mM F^{-} at pH 7(b) consisting of a spin echo control denoted as 'S_0' (top), REDOR experiment denoted as 'S' (middle) and their difference denoted as 'ΔS' (bottom). Spectra were acquired at a spinning rate of 20 kHz, with a π/2 and π pulse (for REDOR experiment) and a pulse delay of 5 s. Synchronous (c) and asynchronous (d) 2D correlation maps generated from 9 to −1 ppm region of the 1H NMR of Hap before and after reacting with 0.25, 1, 10, and 50 mM at pH 7. Red represents a positive correlation, and blue represents a negative correlation. A higher color intensity indicates a stronger positive or negative correlation. (For interpretation of the references to colour in this figure legend, the reader is referred to the web version of this article.)

occurred at pH 7 if this was based on the relationship between F/OH stoichiometry and the F^{-} sorption amount. This result suggests another F sink, e.g., Fap precipitates (motif 3 in Fig. 1), which cannot be explained by the traditional diffusion mechanism.

We propose that an advanced theory of an interface-coupled dissolution-precipitation (ICDP) process [50] could be involved in this reaction. Synchronous and asynchronous 2-dimensional analysis of ^{1}H NMR spectra in Fig. 6a were performed to evaluate the sequential exchange of OH^{-} and F^{-}, and the results are shown in Fig. 6c and d, respectively. The synchronous maps (Fig. 6c) displayed three major autopeaks at 5.8, 1.3, and 0.2 ppm which have been assigned to surface water, OH—F and OH—OH, respectively. Note that autopeaks at the diagonal position represent the overall susceptibility change in peaks intensity influenced by an external perturbation (i.e., F^{-}, here). Cross peaks (off-diagonal peaks) in the synchronous map exhibited correlated signals. The cross peaks showed a negative correlation between peaks at 1.3 and 0.2 ppm, suggesting that the two peaks have an opposing trend with one increasing and the other decreasing. The asynchronous map provides information on the sequential order of signals observed using the spectroscopic technique along the external perturbation (i.e., F^{-}, here). The asynchronous map is antisymmetric with respect to the diagonal line and showed no autopeaks. Specifically, four cross peaks were mainly observed above the diagonal line. The cross peaks at 1.3 and 0.2 ppm are blank in Fig. 6d, suggesting that they change simultaneously.

The ICDP process was also supported by the NanoSIMS analysis. In the NanoSIMS mapping, both depletion and enrichment of the ^{19}F signal were observed at some particles in section 2, 3 and 4 as denoted with arrows. This result indicates that dissolution may occur at one side of the Hap particle. Additionally, we inferred that the dissolution and precipitation processes took place at the same regions.

3.5. Environmental implications

Groundwater, which constitutes 97% of global freshwater, is a vitally important source of drinking water all around the world.

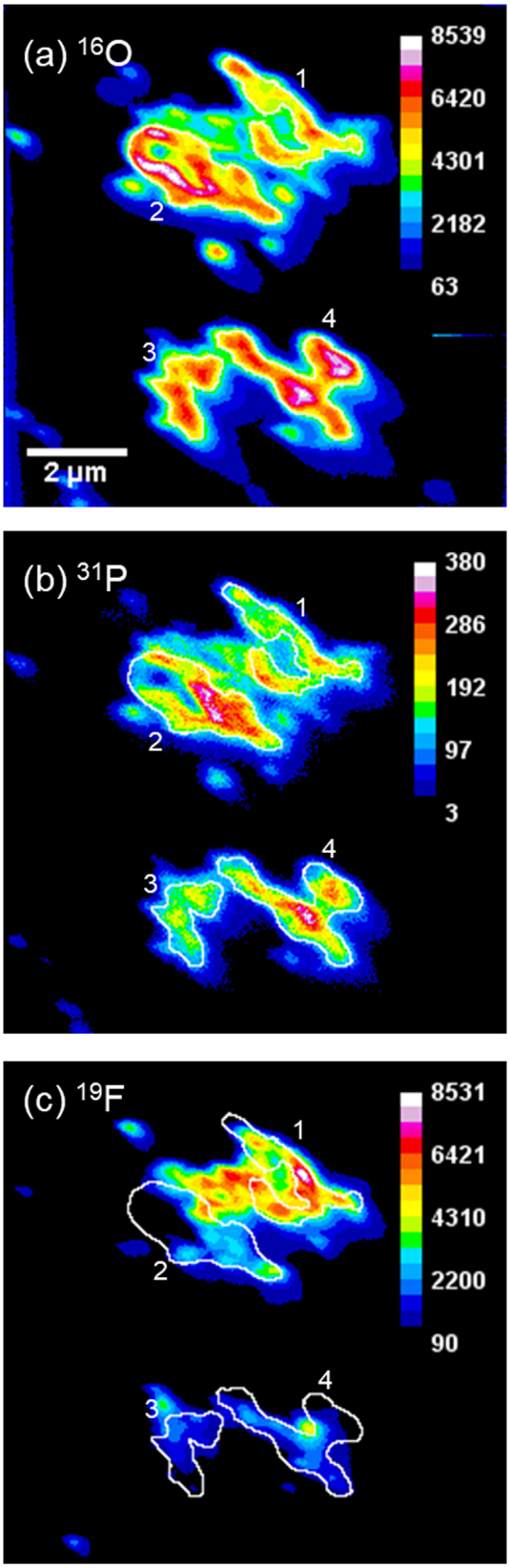

Fig. 7. NanoSIMS ion maps of Hap after reacting with 50 mM F^- shows the distribution of ^{16}O (a), ^{31}P (b) and ^{19}F (c).

In many developing countries and regions, groundwater is the only available and economically viable choice for drinking, such that F-rich groundwater threatens the health of 200 million people in more than 25 nations globally [4]. The findings from this research confirm that Hap-bearing adsorbents are an attractive candidate for F^- removal from groundwater based on the low cost, high efficacy (>21 mg/g), and stability (see Fig. S10 for its resistance against competing anions). Our study has provided strong experimental evidence that the formation of Fap is the dominant mechanism for F^- sorption by Hap under conditions for treating most natural F^- contaminated groundwater (Fig. 4). This finding provides a theoretical basis for the regeneration of this material by rinsing in 1 M NaOH (Scheme 1), showing that Hap has strong regenerative capacity (Fig. 8). After four regeneration cycles, Hap can still remove up to 90% of dissolved F (0.5 mM initial [F^-]) and meet the WHO drinking water standard for F^- (1.5 mg/L). In addition, the variable temperature experiments (Fig. S11) showed that Hap remains effective at elevated temperature (40 °C), which ensures the efficient application of Hap material in tropical and subtropical regions such as India and eastern Africa.

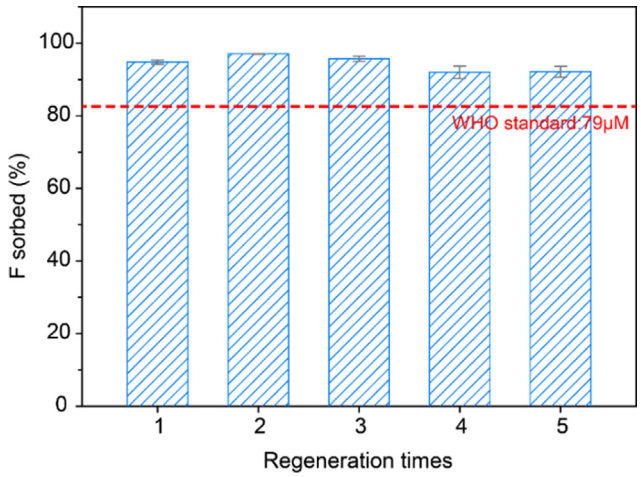

Fig. 8. Fluoride sorption capacity of Hap at pH 7 and an initial F^- concentration of 0.5 mM after successive cycles of regeneration by suspension in 1 M NaOH solution.

4. Conclusions

In this study, we systematically characterized the F environment during its uptake by Hap. The results obtained from ^{19}F solid-state NMR spectroscopy, FTIR, and NanoSIMS revealed the presence of the two main products at distinct pH-dependent concentrations, that is, CaF_2 precipitates at high [F^-] and Fap-like products at low [F^-]. This confirms that Hap is a potential natural material for defluoridation with low-cost, high efficiency (>21 mg F/g at pH 7) and strong regenerative capacity. Considering that the pH of natural groundwater for human consumption is between 6.5 and 8.5 (according to the WHO) and that the fluoride concentration is below 50 mg/L, we demonstrate that Fap is the prime product at natural groundwater. From a theoretical perspective, the heterogeneous distribution of F^- ions mapped by Nano Secondary Ion Mass Spectrometry (NanoSIMS) indicate that the interfacial coupled dissolution-precipitation process (ICDP) plays an important role in F uptake by Hap [50]. Overall, these results provide deep insight into the nature of F^- uptake by calcium-based sorbents in aqueous environments.

Acknowledgements

We appreciate the constructive comments from anonymous reviewers and the editor. We also greatly thank Dr. Hao Jialong at the Institute of Geology and Geophysics of the Chinese Academy

of Sciences for assistance in the NanoSIMS analysis. This research was funded by the National Natural Science Foundation of China (NSFC) (Grant No. 41722303) and the Outstanding Young Scientists Program sponsored by the Natural Science Foundation of Jiangsu Province of China (BK20150018). Wei Li is grateful for the financial support for Start-Up from Nanjing University and the 1000 Youth Talent Program sponsored by the Chinese central government for purchase of the solid-state NMR facility.

Appendix A. Supplementary material

Supplementary data to this article can be found online at https://doi.org/10.1016/j.jcis.2019.09.039.

References

[1] S. Ayoob, A.K. Gupta, V.T. Bhat, A conceptual overview on sustainable technologies for the defluoridation of drinking water, Crit. Rev. Environ. Sci. Technol. 38 (2008) 401–470.
[2] M.C. Smith, E.M. Lantz, H.V. Smith, The cause of mottled enamel, Science 74 (1931) 244.
[3] F.L. Theiss, S.J. Couperthwaite, G.A. Ayoko, R.L. Frost, A review of the removal of anions and oxyanions of the halogen elements from aqueous solution by layered double hydroxides, J. Colloid Interf. Sci. 417 (2014) 356–368.
[4] S. Ayoob, A.K. Gupta, Fluoride in drinking water: a review on the status and stress effects, Crit. Rev. Environ. Sci. Technol. 36 (2006) 433–487.
[5] J. Fawell, K. Bailey, J. Chilton, E. Dahi, L. Fewtrell, Y. Magara, Fluoride in Drinking Water, World Health Organization, London, UK, 2006.
[6] H.R.J. Frederick, R.D. Woosley, The removal of excess fluoride from drinking water by activated alumina, J. Am. Water Works Ass. 71 (1979) 45–49.
[7] M.S. Onyango, Y. Kojima, O. Aoyi, E.C. Bernardo, H. Matsuda, Adsorption equilibrium modeling and solution chemistry dependence of fluoride removal from water by trivalent-cation-exchanged zeolite F-9, J. Colloid Interface Sci. 279 (2004) 341–350.
[8] D.S. Bhagava, D.L. Killedar, Fluoride adsorption on fishbone charcoal through a moving media adsoeber, Water Res. 26 (1992) 781–788.
[9] R. Sivabalan, S. Rengaraj, B. Arabindoo, V. Murugesan, Cashewnut sheath carbon: a new sorbent for defluoridation of water, Ind. J. Chem. Technol. 10 (2003) 217–222.
[10] X. Fan, D.J. Parker, M.D. Smith, Adsorption kinetics of fluoride on low cost materials, Water Res. 37 (2003) 4929–4937.
[11] M. Srimurali, A. Pragathi, J. Karthikeyan, A study on removal of fluorides from drinking water by adsorption onto low-cost materials, Environ. Pollut. 99 (1998) 285–289.
[12] M. Mahramanlioglu, I. Kizilcikli, I.O. Bicer, Adsorption of fluoride from aqueous solution by acid treated spent bleaching earth, J. Fluor. Chem. 115 (2002) 41–47.
[13] Y. Çengeloğlu, E. Kır, M. Ersöz, Removal of fluoride from aqueous solution by using red mud, Sep. Purif. Technol. 28 (2002) 81–86.
[14] C.S. Sundaram, N. Viswanathan, S. Meenakshi, Defluoridation chemistry of synthetic hydroxyapatite at nano scale: equilibrium and kinetic studies, J. Hazard. Mater. 155 (2008) 206–215.
[15] S. Gao, R. Sun, Z. Wei, H. Zhao, H. Li, F. Hu, Size-dependent defluoridation properties of synthetic hydroxyapatite, J. Fluor. Chem. 130 (2009) 550–556.
[16] S. Gao, J. Cui, Z. Wei, Study on the fluoride adsorption of various apatite materials in aqueous solution, J. Fluor. Chem. 130 (2009) 1035–1041.
[17] C.S. Sundaram, N. Viswanathan, S. Meenakshi, Fluoride sorption by nano-hydroxyapatite/chitin composite, J. Hazard. Mater. 172 (2009) 147–151.
[18] M. Jiménez-Reyes, M. Solache-Ríos, Sorption behavior of fluoride ions from aqueous solutions by hydroxyapatite, J. Hazard. Mater. 180 (2010) 297–302.
[19] V. Sternitzke, R. Kaegi, J.N. Audinot, E. Lewin, J.G. Hering, C.A. Johnson, Uptake of fluoride from aqueous solution on nano-sized hydroxyapatite: examination of a fluoridated surface layer, Environ. Sci. Technol. 46 (2012) 802–809.
[20] W. Li, A.M. Pierre-Louis, K.D. Kwon, J.D. Kubicki, D.R. Strongin, B.L. Phillips, Molecular level investigations of phosphate sorption on corundum (α-Al2O3) by 31P solid state NMR, ATR-FTIR and quantum chemical calculation, Geochim. Cosmochim. Acta 107 (2013) 252–266.
[21] C.M. Kanno, R.L. Sanders, S.M. Flynn, G. Lessard, S.C.B. Myneni, Novel apatite-based sorbent for defluoridation: synthesis and sorption characteristics of nano-micro-crystalline hydroxyapatite-coated-limestone, Environ. Sci. Technol. 48 (2014) 5798–5807.
[22] M.J. Mobley, J.P. Yesinowski, The fluoride-hydroxyapatite reaction studied by F-19 magic-angle spinning NMR, J. Dental Res. 62 (1983) 301.
[23] J.P. Yesinowski, M.J. Mobley, F-19 MAS-NMR of fluoridated hydroxyapatite surfaces, J. Am. Chem. Soc. 105 (1983) 6191–6193.
[24] D.J. White, W.D. Bowman, R.V. Faller, M.J. Mobley, R.A. Wolfgang, J.P. Yesinowski, F-19 MAS-NMR and solution chemical characterization of the reactions of fluoride with hydroxyapatite and powdered enamel, Acta Odontol. Scand. 46 (1988) 375–389.
[25] W. Li, J. Feng, K.D. Kwon, J.D. Kubicki, B.L. Phillips, Surface speciation of phosphate on boehmite (γ-AlOOH) determined from NMR spectroscopy, Langmuir 26 (2010) 4753–4761.
[26] J. Lin, S. Raghavan, D.W. Fuerstenau, The adsorption of fluoride ions by hydroxyapatite from aqueous solution, Colloids Surf. 3 (1981) 357–370.
[27] K.J. Farly, D.A. Dzombak, F.M.M. Morel, A surface precipitation model for the sorption of cations on metal oxides, J. Colloid Interface Sci. 106 (1985) 226–241.
[28] A. Yehia, K. Ezzat, Fluoride ion uptake by synthetic apatites, Adsorp. Sci. Technol. 27 (2009) 337–347.
[29] J. Chen, Z. Yu, P. Zhu, J. Wang, Z. Gan, J. Wei, Y. Zhao, S. Wei, Effects of fluorine on the structure of fluorohydroxyapatite: a study by XRD, solid-state NMR and Raman spectroscopy, J. Mater. Chem. B 3 (2015) 34–38.
[30] J. Christoffersen, M.R. Christoffersen, J. Arends, E.S. Leonardsen, Formation of phosphate-containing calcium fluoride at the expense of enamel, hydroxyapatite and fluorapatite, Caries. Res. 29 (1995) 223–230.
[31] L. Xu, T. Zheng, S. Yang, L. Zhang, J. Wang, W. Liu, L. Chen, J. Diwu, Z. Chai, S. Wang, Uptake mechanisms of Eu(III) on hydroxyapatite: a potential permeable reactive barrier backfill material for trapping trivalent minor actinides, Environ. Sci. Technol. 50 (2016) 3852–3859.
[32] N.R. Mohammed, N.W. Kent, R.J.M. Lynch, N. Karpukhina, R. Hill, P. Anderson, Effects of fluoride on in vitro enamel demineralization analyzed by 19F MAS-NMR, Caris Res. 47 (2013) 421–428.
[33] M. Currell, I. Cartwright, M. Raveggi, D. Han, Controls on elevated fluoride and arsenic concentrations in groundwater from the Yuncheng Basin, China, Appl. Geochem. 26 (2011) 540–552.
[34] J. He, Y. An, F. Zhang, Geochemical characteristics and fluoride distribution in the groundwater of the Zhangye Basin in Northwestern China, J. Geochem. Explor. 135 (2013) 22–30.
[35] S. Hu, T. Luo, C. Jing, Principal component analysis of fluoride geochemistry of groundwater in Shanxi and Inner Mongolia, China, J. Geochem. Explor. 135 (2013) 124–129.
[36] X. Li, X. Hou, Z. Zhou, Geochemical provenance and spatial distribution of fluoride in groundwater of Taiyuan basin, China, Environ. Earth Sci. 62 (2011) 1635–1642.
[37] P.R. Salve, A. Maurya, P.S. Kumbhare, D.S. Ramteke, S.R. Wate, Assessment of groundwater quality with respect to fluoride, B. Environ. Contam. Tox. 81 (2008) 289–293.
[38] P.L. Smedley, M. Zhang, G. Zhang, Z. Luo, Mobilisation of arsenic and other trace elements in fluviolacustrine aquifers of the Huhhot Basin, Inner Mongolia, Appl. Geochem. 18 (2003) 1453–1477.
[39] C. Su, Y. Wang, X. Xie, J. Li, Aqueous geochemistry of high-fluoride groundwater in Datong Basin, Northern China, J. Geochem. Explor. 135 (2013) 79–92.
[40] C. Vikas, R. Kushwaha, M.K. Pandit, Hydrochemical status of groundwater in District Ajmer (NW India) with reference to fluoride distribution, J. Geol. Soc. India 73 (2009) 773–784.
[41] C. Vikas, R. Kushwaha, W. Ahmad, V. Prasannakumar, R. Reghunath, Genesis and geochemistry of high fluoride bearing groundwater from a semi-arid terrain of NW India, Environ. Earth Sci. 68 (2013) 289–305.
[42] A.T. Kreinbrink, C.D. Sazavsky, J.W. Pyrz, D.G.A. Nelson, R.S. Honkonen, Fast-Magic-Angle-Spinning 19F NMR of inorganic fluorides and fluoridated apatitic surfaces, J. Magnet. Reson. 88 (1990) 267–276.
[43] J.S. Vaughn, D.H. Lindsley, H. Nekvasil, J.M. Hughes, B.L. Phillips, Complex F, Cl apatite solid solution investigated using multinuclear solid state NMR methods, J. Phy. Chem. C 122 (2017) 530–539.
[44] J.S. Vaughn, W.R. Woerner, D.H. Lindsley, H. Nekvasil, J.M. Hughes, B.L. Phillips, Hydrogen environments in low-OH, F, Cl apatites revealed by double resonance solid-state NMR, J. Phys. Chem. C 119 (2015) 28605–28613.
[45] J.P. Yesinowski, H. Eckert, Hydrogen environments in calcium phosphates: proton MAS NMR at high spinning speeds, J. Am. Chem. Soc. 109 (1987) 6274–6282.
[46] M. Jarlbring, D.E. Sandstrom, O.N. Antzutkin, W. Forsling, Characterization of active phosphorus surface sites at synthetic carbonate-free fluorapatite using single-pulse 1H, 31P, and 31P CP MAS NMR, Langmuir 22 (2006) 4787–4792.
[47] R.D. Shannon, Revised effective ionic radii and systematic studies of interatomic distances in halides and chalcogenides, Acta Crystallogr. 32 (1976) 751–767.
[48] J.M. Hugh, J. Rakovan, The crystal structure of apatite, Ca5(PO4)3(F, OH, Cl), Rev. Miner. Geochem. 48 (2002) 1–12.
[49] Å. Bengtsson, A. Shchukarev, P. Persson, S. Sjöberg, Phase transformations, ion-exchange, adsorption, and dissolution processes in aquatic fluorapatite systems, Langmuir 25 (2009) 2355–2362.
[50] E. Ruiz-Agudo, C.V. Putnis, A. Putnis, Coupled dissolution and precipitation at mineral-fluid interface, Chem. Geol. 383 (2014) 132–146.